Hybrid natural element method for large deformation elastoplasticity problems*

Ma Yong-Qi(马永其)[a)b)†] and Zhou Yan-Kai(周延凯)[a)]

[a)] *Shanghai Institute of Applied Mathematics and Mechanics, Shanghai University, Shanghai* 200072, *China*
[b)] *Department of Mechanics, Shanghai University, Shanghai* 200444, *China*

(Received 5 October 2014; revised manuscript received 21 October 2014; published online 30 January 2015)

We present the hybrid natural element method (HNEM) for two-dimensional elastoplastic large deformation problems. Sibson interpolation is adopted to construct the shape functions of nodal incremental displacements and incremental stresses. The incremental form of Hellinger–Reissner variational principle for elastoplastic large deformation problems is deduced to obtain the equation system. The total Lagrangian formulation is used to describe the discrete equation system. Compared with the natural element method (NEM), the HNEM has higher computational precision and efficiency in solving elastoplastic large deformation problems. Some numerical examples are selected to demonstrate the advantage of the HNEM for large deformation elastoplasticity problems.

Keywords: hybrid natural element method, large deformation elastoplasticity, Hellinger–Reissner variational principle, meshless method

PACS: 02.60.Cb, 02.60.Lj, 46.15.–x **DOI:** 10.1088/1674-1056/24/3/030204

1. Introduction

In solving the large deformation problems, the finite element method (FEM) may encounter difficulties when adaptive meshing or rezoning techniques may be helpful, but they are not widely used because of their complexity and imperfections. On the contrary, the meshless method is a numerical method based on nodes, which does not need to generate mesh, so adaptive meshing or rezoning techniques are not used in the meshless method.[1] Therefore, the meshless method has some advantages in handling large deformation problems.

Many meshless methods have been developed, such as the element-free Galerkin method,[2–4] improved element-free Galerkin method,[5–8] complex variable meshless method,[9–11] complex variable element-free Galerkin method,[12–16] interpolating element-free Galerkin method,[17,18] radial basis function method,[19] finite point method,[20,21] meshless local Petrov–Galerkin method,[22] reproducing kernel particle method,[23–27] meshless manifold method,[28,29] boundary element-free method,[30–38] and the improved boundary element-free method.[39–42]

Braun and Sambridge presented another meshless method, namely, the natural element method.[43] Many researchers applied the NEM to solve mechanical problems. Sukumar *et al.*[44] used the NEM to analyze two-dimensional small displacement elastostatics. Bueche *et al.*[45] investigated the performance of NEM in two-dimensional linear elastodynamics. Cueto *et al.*[46] employed the NEM for two-dimensional and three-dimensional piece-wise homogeneous domains. Martínez *et al.*[47] simulated flows involving short fiber suspensions with the NEM. Calvo *et al.*[48] solved large strain hyperelastic problems using the NEM. Daneshmand and Niroomandi discussed the vibration modes of fluid-structure systems with the NEM.[49] Daneshmand *et al.*[50] calculated two-dimensional flow under sluice gates using the NEM. Shahrokhabadi *et al.*[51] developed the NEM to solve seepage problems. Cho *et al.*[52] established the NEM of Reissner–Mindlin plate for a locking-free numerical analysis of plate-like thin elastic structures. Different from the NEM, the HNEM adopts displacement approximation and stresses approximation respectively to obtain the discrete equation system with the Hellinger–Reissner variational principle. The HNEM has been used to solve the elasticity problems and elastoplastic problems.[53,54]

Various meshless methods have been developed for large deformation analysis of non-linear materials and structures. Chen *et al.*[55] analyzed non-linear elastic and inelastic structures based on reproducing kernel particle methods. Li *et al.*[56] studied mesh-free simulations of shear banding in large deformation. Ren *et al.*[57] modelled the superelastic behaviour of shape memory alloys using the element-free Galerkin method. Liew *et al.*[58] analyzed the pseudoelastic behavior of an SMA beam by the element-free Galerkin method. Liew *et al.*[59] developed an FSDT and a meshfree method for corrugated plates. Naffa and Al-Gahtani discussed the radial basis function method for large deflection of thin plates.[60] Rossi and Alves investigated a modified element-free Galerkin method and applied it to large deformation processes.[61] Zhao and Liew applied the element-free kp-Ritz method to functionally graded plates.[62] Doweidar *et al.*[63] adopted the implicit and explicit natural element methods to

*Project supported by the Natural Science Foundation of Shanghai, China (Grant No. 13ZR1415900).
†Corresponding author. E-mail: mayq@staff.shu.edu.cn
© 2015 Chinese Physical Society and IOP Publishing Ltd

analyze large strains of soft biological tissues. Li *et al.*[64–66] proposed complex variable element-free Galerkin methods for large deformation problems. Peng *et al.*[67] used the FSDT and the moving least-squares approximation to analyze ribbed rectangular plates.

Based on the Sibson interpolation, the HNEM for two-dimensional elastoplastic large deformation problems is discussed in this paper. The incremental formulation of the Hellinger–Reissner variational principle is deduced to obtain the incremental equation system. The total Lagrangian formulation is used to describe this equation system. The Mises yield criterion is adopted as yield condition and the linear hardening elastoplastic model is used as the flow rule. The corresponding formulae are solved by the Newton–Raphson iteration method with displacement convergence criterion. Some numerical examples of large deformation elastoplasticity problems are computed by the HNEM.

2. Basic equations of large deformation elastoplasticity problems

2.1. Incremental formulation of Hellinger–Reissner variational principle for large deformation elastoplasticity problems

We adopt the total Lagrangian formulation to describe the large deformation problems, i.e., the original configuration is used as reference configuration. For a question domain ${}^0\Omega$, suppose that displacement ${}^t_0u_i$, strain ${}^t_0\varepsilon_{ij}$, and stress ${}^t_0\sigma_{ij}$ at time t have been obtained, and body force ${}^{t+\Delta t}_0\bar{f}_i$ on ${}^0\Omega$, boundary force ${}^{t+\Delta t}_0\bar{t}_i$ on ${}^0\Gamma_\sigma$, and boundary displacement ${}^{t+\Delta t}_0\bar{u}_i$ on ${}^0\Gamma_u$ at time $t+\Delta t$ are given. Then displacement ${}^{t+\Delta t}_0u_i$, strain ${}^{t+\Delta t}_0\varepsilon_{ij}$, and stress ${}^{t+\Delta t}_0\sigma_{ij}$ at time $t+\Delta t$ can be obtained after incremental displacement ${}_0u_i$, incremental strain ${}_0\varepsilon_{ij}$, and incremental stress ${}_0\sigma_{ij}$ are computed from t to $t+\Delta t$.

The incremental formulation of the Hellinger–Reissner variational principle can be expressed as[68]

$$\begin{aligned}\prod_{\rm HR} = &\int_{{}_0\Omega}\left[-B+\left({}^t_0\sigma_{ij}+{}_0\sigma_{ij}\right){}_0\varepsilon_{ij}\right]{}^0\mathrm{d}\Omega\\ &-\int_{{}_0\Omega}{}^{t+\Delta t}_0\bar{f}_{i0}u_i{}^0\mathrm{d}\Omega-\int_{{}_0\Gamma_\sigma}{}^{t+\Delta t}_0\bar{t}_{i0}u_i{}^0\mathrm{d}\Gamma\\ &-\int_{{}_0\Gamma_u}{}^{t+\Delta t}_0\bar{t}_i\left({}_0u_i-{}_0\bar{u}_i\right){}^0\mathrm{d}\Gamma,\end{aligned}\tag{1}$$

where B is the incremental surplus energy density function

$$B=\frac{1}{2}{}_0C_{ijkl0}\sigma_{ij0}\sigma_{kl},\tag{2}$$

with ${}_0C_{ijkl}$ being the relationship between stress increment ${}_0\sigma_{ij}$ and strain increment ${}_0\varepsilon_{ij}$,

$${}_0\varepsilon_{ij}={}_0C_{ijkl0}\sigma_{kl}.\tag{3}$$

It must be pointed out that the linear relationship supposed here is true only for an infinitesimal increment.

The decomposition of incremental strain ${}_0\varepsilon_{ij}$ can be written as

$${}_0\varepsilon_{ij}={}_0e_{ij}+{}_0\eta_{ij},\tag{4}$$

where ${}_0e_{ij}$ and ${}_0\eta_{ij}$ are the linear and quadratic terms of the incremental strain ${}_0\varepsilon_{ij}$, respectively. Namely,

$${}_0e_{ij}={}_0e^{(\mathrm{L1})}_{ij}+{}_0e^{(\mathrm{L2})}_{ij},\tag{5}$$

$${}_0\eta_{ij}=\frac{1}{2}{}_0u_{k,i0}u_{k,j},\tag{6}$$

where

$${}_0e^{(\mathrm{L1})}_{ij}=\frac{1}{2}\left({}_0u_{i,j}+{}_0u_{j,i}\right),\tag{7}$$

$${}_0e^{(\mathrm{L2})}_{ij}=\frac{1}{2}\left({}^t_0u_{k,i0}u_{k,j}+{}^t_0u_{k,j0}u_{k,i}\right).\tag{8}$$

Then equation (1) can be rewritten as

$$\begin{aligned}\prod_{\rm HR} = &\int_{{}_0\Omega}-\frac{1}{2}{}_0C_{ijkl0}\sigma_{ij0}\sigma_{kl}{}^0\mathrm{d}\Omega\\ &+\int_{{}_0\Omega}{}_0\sigma_{ij0}e_{ij}{}^0\mathrm{d}\Omega+\int_{{}_0\Omega}{}_0\sigma_{ij0}\eta_{ij}{}^0\mathrm{d}\Omega\\ &+\int_{{}_0\Omega}{}^t_0\sigma_{ij0}e_{ij}{}^0\mathrm{d}\Omega+\int_{{}_0\Omega}{}^t_0\sigma_{ij0}\eta_{ij}{}^0\mathrm{d}\Omega\\ &-\int_{{}_0\Omega}{}^{t+\Delta t}_0\bar{f}_{i0}u_i{}^0\mathrm{d}\Omega-\int_{{}_0\Gamma_\sigma}{}^{t+\Delta t}_0\bar{t}_0u_i{}^0\mathrm{d}\Gamma\\ &-\int_{{}_0\Gamma_u}{}^{t+\Delta t}_0\bar{t}\left({}_0u_i-{}_0\bar{u}_i\right){}^0\mathrm{d}\Gamma.\end{aligned}\tag{9}$$

For further linearization, ${}_0\sigma_{ij0}\eta_{ij}$ in the third integral term in Eq. (9) needs to be omitted. Suppose the displacement boundary condition was satisfied, then equation (9) can be rewritten as

$$\begin{aligned}\prod_{\rm HR} = &\int_{{}_0\Omega}-\frac{1}{2}{}_0C_{ijkl0}\sigma_{ij0}\sigma_{kl}{}^0\mathrm{d}\Omega+\int_{{}_0\Omega}{}_0\sigma_{ij0}e_{ij}{}^0\mathrm{d}\Omega\\ &+\int_{{}_0\Omega}{}^t_0\sigma_{ij0}e_{ij}{}^0\mathrm{d}\Omega+\int_{{}_0\Omega}{}^t_0\sigma_{ij0}\eta_{ij}{}^0\mathrm{d}\Omega\\ &-\int_{{}_0\Omega}{}^{t+\Delta t}_0\bar{f}_{i0}u_i{}^0\mathrm{d}\Omega-\int_{{}_0\Gamma_\sigma}{}^{t+\Delta t}_0\bar{t}_0u_i{}^0\mathrm{d}\Gamma.\end{aligned}\tag{10}$$

Thus, the incremental formulation of the Hellinger–Reissner variational principle to deduce the HNME for large deformation elastoplasticity problems is found.

2.2. Two-dimensional elastoplastic constitution relationship

For an isotropic hardening material, the incremental form of the stress–strain relation in plane problems can be expressed as

$${}_0\varepsilon={}_0C_0\sigma=\begin{cases}{}_0C^{\mathrm{e}}{}_0\sigma, & \text{in elastic state,}\\ {}_0C^{\mathrm{ep}}{}_0\sigma, & \text{in plastic state.}\end{cases}\tag{11}$$

We adopt the Mises yield criterion to judge whether an arbitrary point of the material is in the plastic state. When equivalent stress σ_l of a point is greater than yield stress σ_{s} of the material, then this point is in plastic state; otherwise it is in

elastic state. The equivalent stress σ_l of an arbitrary point can be written as

$$\sigma_l = \begin{cases} \sqrt{\sigma_{11}^2 + \sigma_{22}^2 - \sigma_{11}\sigma_{22} + 3\sigma_{12}^2}, & \text{plane stress}, \\ \sqrt{\dfrac{3}{4}(\sigma_{11} - \sigma_{22})^2 + 3\sigma_{12}^2}, & \text{plane strain}. \end{cases} \tag{12}$$

If the point is in elastic state, ${}_0\boldsymbol{C}^{\mathrm{e}}$ of this point is

$$({}_0\boldsymbol{C}^{\mathrm{e}})^{-1} = \frac{\bar{E}}{(1-\bar{\nu}^2)} \begin{bmatrix} 1 & \bar{\nu} & 0 \\ \bar{\nu} & 1 & 0 \\ 0 & 0 & \dfrac{1-\bar{\nu}}{2} \end{bmatrix}, \tag{13}$$

where

$$\bar{E} = \begin{cases} E, & \text{plane stress}, \\ \dfrac{E}{1-\nu^2}, & \text{plane strain}, \end{cases} \tag{14}$$

$$\bar{\nu} = \begin{cases} \nu, & \text{plane stress}, \\ \dfrac{\nu}{1-\nu}, & \text{plane strain}. \end{cases} \tag{15}$$

When the point is in the plastic state, for plane stress problems, ${}_0\boldsymbol{C}^{\mathrm{ep}}$ of this point is

$$({}_0\boldsymbol{C}^{\mathrm{ep}})^{-1} = \frac{E}{Q_\sigma} \begin{bmatrix} S_{22}^2 + 2P_\sigma & -S_{11}S_{22} + 2\nu P_\sigma & -\dfrac{S_{11} + \nu S_{22}}{1+\nu}\sigma_{12} \\ -S_{11}S_{22} + 2\nu P_\sigma & S_{11}^2 + 2P_\sigma & -\dfrac{S_{22} + \nu S_{11}}{1+\nu}\sigma_{12} \\ -\dfrac{S_{11} + \nu S_{22}}{1+\nu}\sigma_{12} & -\dfrac{S_{22} + \nu S_{11}}{1+\nu}\sigma_{12} & \dfrac{R_\sigma}{2(1+\nu)} + \dfrac{2H'}{9E}(1-\nu)\sigma_l^2 \end{bmatrix}, \tag{16}$$

and for plane strain problems, ${}_0\boldsymbol{C}^{\mathrm{ep}}$ of this point is

$$({}_0\boldsymbol{C}^{\mathrm{ep}})^{-1} = \frac{E}{1+\nu} \begin{bmatrix} \dfrac{1-\nu}{1-2\nu} - \omega S_{11}^2 & \dfrac{\nu}{1-2\nu} - \omega S_{11}S_{22} & -\omega S_{11}\sigma_{12} \\ \dfrac{\nu}{1-2\nu} - \omega S_{11}S_{22} & \dfrac{1-\nu}{1-2\nu} - \omega S_{22}^2 & -\omega S_{22}\sigma_{12} \\ -\omega S_{11}\sigma_{12} & -\omega S_{22}\sigma_{12} & \dfrac{1}{2} - \omega\sigma_{12}^2 \end{bmatrix}, \tag{17}$$

where E is Young's modulus, ν is Poisson's ratio, and H' is the plastic modulus for material hardening, and

$$H' = \frac{EE'}{E - E'}, \tag{18}$$

E' is known as the tangent modulus. S_{11} and S_{22} are the deviatoric stresses, and

$$S_{11} = \begin{cases} \sigma_{11} - \dfrac{\sigma_{11} + \sigma_{22}}{3}, & \text{plane stress}, \\ \sigma_{11} - \dfrac{\sigma_{11} + \sigma_{22}}{2}, & \text{plane strain}, \end{cases} \tag{19}$$

$$S_{22} = \begin{cases} \sigma_{22} - \dfrac{\sigma_{11} + \sigma_{22}}{3}, & \text{plane stress}, \\ \sigma_{22} - \dfrac{\sigma_{11} + \sigma_{22}}{2}, & \text{plane strain}. \end{cases} \tag{20}$$

In Eqs. (16) and (17),

$$P_\sigma = \frac{2H'}{9E}\sigma_l^2 + \frac{\sigma_{12}^2}{1+\nu}, \tag{21}$$

$$R_\sigma = S_{11}^2 + 2\nu S_{11}S_{22} + S_{22}^2, \tag{22}$$

$$Q_\sigma = R_\sigma + 2(1-\nu^2)P_\sigma, \tag{23}$$

$$\omega = \frac{9G}{2\sigma_l^2(H' + 3G)}, \tag{24}$$

$$G = \frac{E}{2(1+\nu)}. \tag{25}$$

3. The HNEM for elastoplastic large deformation problems

3.1. Sibson interpolation

The Sibson interpolation is based on the well-known Voronoi diagram and Delaunay tessellation. Suppose a set of scattered nodes $N = \{N_1, N_2, \ldots, N_m\}$ in $\boldsymbol{R}^2$, the nodal coordinates are $\boldsymbol{x}_i$ $(i = 1, 2, \ldots, m)$. The Voronoi diagram $T(N)$ of the set N is a subdivision of the domain into Voronoi cells $T(N_i)$, and the Voronoi cell $T(N_i)$ is defined as

$$T(N_i) = \{\boldsymbol{x} \in R^2 \,|\, d(\boldsymbol{x}, \boldsymbol{x}_i) < d(\boldsymbol{x}, \boldsymbol{x}_j), \forall j \neq i\}, \tag{26}$$

where $d(\boldsymbol{x}_i, \boldsymbol{x}_j)$ is the distance between $\boldsymbol{x}_i$ and $\boldsymbol{x}_j$. The Delaunay triangulation is the dual of the Voronoi diagram, which is constructed by connecting the nodes whose Voronoi cells have common boundaries. The circumcircles of Delaunay triangles, known as natural neighbour circumcircles, can be used to find the natural neighbour nodes of $\boldsymbol{x}$. In other words, if $\boldsymbol{x}$ lies within the natural neighbour circumcircle of triangle $\mathrm{DT}(N_i, N_j, N_k)$, then N_i, N_j, and N_k are the natural neighbour nodes of $\boldsymbol{x}$. The Voronoi diagram, the Delaunay triangulation, and natural neighbour circumcircles of a set N are shown in Fig. 1, in which we can find that nodes 1, 5, 6, 7 are the natural neighbor nodes of $\boldsymbol{x}$.

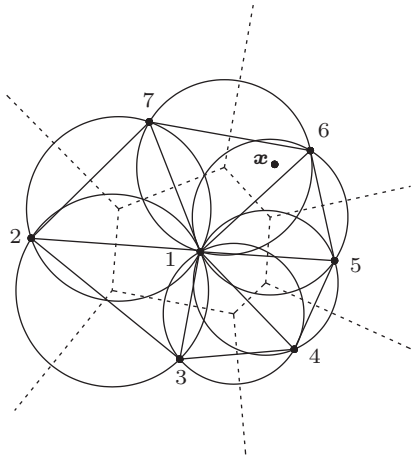


Fig. 1. Voronoi diagram $T(N)$, Delaunay triangulation DT(N), and natural neighbour circumcircles.

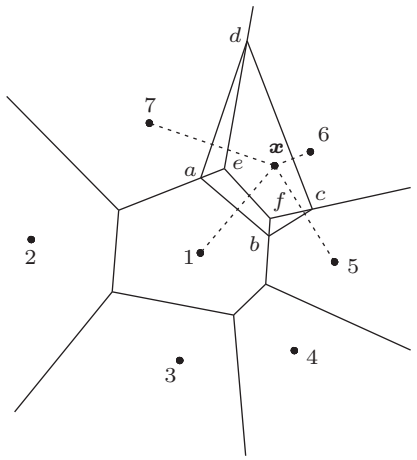


Fig. 2. Voronoi cell $T(\boldsymbol{x})$.

The Sibson interpolation shape function of $\boldsymbol{x}$ with respect to a natural neighbour $\boldsymbol{x}_i$ is defined as

$$\phi_i(\boldsymbol{x}) = \frac{A_i(\boldsymbol{x})}{A(\boldsymbol{x})}, \tag{27}$$

$$A(\boldsymbol{x}) = \sum_{j=1}^{n} A_j(\boldsymbol{x}), \tag{28}$$

where n is the number of natural neighbours of $\boldsymbol{x}$, $A_i(\boldsymbol{x})$ is the area of overlap of Voronoi cell $T(\boldsymbol{x}_i)$ and Voronoi cell $T(\boldsymbol{x})$, and $A(\boldsymbol{x})$is the area of Voronoi cell $T(\boldsymbol{x})$.

Referring to Fig. 2, the Sibson interpolation shape function $\phi_5(\boldsymbol{x})$ is

$$\phi_5(\boldsymbol{x}) = \frac{A_{bcf}}{A_{abcd}}. \tag{29}$$

The derivatives of the shape functions can be obtained by differentiating Eq. (27)

$$\phi_{i,j}(\boldsymbol{x}) = \frac{A_{i,j}(\boldsymbol{x}) - \phi_i(\boldsymbol{x})A_{,j}(\boldsymbol{x})}{A(\boldsymbol{x})}, \quad (j = 1,2). \tag{30}$$

The displacement approximations $\boldsymbol{u}^{\mathrm{h}}(\boldsymbol{x})$ of point $\boldsymbol{x}$ can be expressed as

$$\boldsymbol{u}^{\mathrm{h}}(\boldsymbol{x}) = \sum_{i=1}^{n} \phi_i(\boldsymbol{x})\boldsymbol{u}_i, \tag{31}$$

where $\boldsymbol{u}_i$ is the displacement vector of node i.

According to definition of the shape function (27), the following remarkable properties is self-evident:

$$0 \le \phi_i(x) \le 1, \tag{32}$$

$$\phi_i(\boldsymbol{x}_j) = \delta_{ij} \tag{33}$$

$$\sum_{i=1}^{n} \phi_i(\boldsymbol{x}) = 1, \tag{34}$$

$$\boldsymbol{x} = \sum_{i=1}^{n} \phi_i(\boldsymbol{x})\boldsymbol{x}_i. \tag{35}$$

Equation (33) shows that the shape functions possess the Kronecker delta function property, therefore the essential boundary conditions can be implemented directly as in the FEM. Equations (34) and (35) define a partition of unity and linear completeness, which imply that the shape functions can reproduce the rigid body displacement and the constant strain.

3.2. The HNEM for two-dimensional elastoplastic large deformation problems

Suppose there are n nodes in the two-dimensional solution domain ${}^0\Omega$, from Sibson interpolation approximations (Eq. (31)), the incremental displacement vector ${}_0\boldsymbol{u}(\boldsymbol{x})$ and the incremental stress vector ${}_0\boldsymbol{\sigma}(\boldsymbol{x})$ from t to $t+\Delta t$ at any point $\boldsymbol{x}$ in the domain ${}^0\Omega$ can be written as

$${}_0\boldsymbol{u}(\boldsymbol{x}) = {}_0\boldsymbol{\Phi}(\boldsymbol{x})\,{}_0\boldsymbol{q}, \tag{36}$$

$${}_0\boldsymbol{\sigma}(\boldsymbol{x}) = {}_0\boldsymbol{P}(\boldsymbol{x})\,{}_0\boldsymbol{\beta}, \tag{37}$$

where ${}_0\boldsymbol{\Phi}(\boldsymbol{x})$ and ${}_0\boldsymbol{P}(\boldsymbol{x})$ are the matrix form of shape functions

$${}_0\boldsymbol{\Phi}(\boldsymbol{x}) = \left({}_0\boldsymbol{\Phi}_1(\boldsymbol{x}), {}_0\boldsymbol{\Phi}_2(\boldsymbol{x}), \ldots, {}_0\boldsymbol{\Phi}_n(\boldsymbol{x})\right), \tag{38}$$

$${}_0\boldsymbol{\Phi}_i(\boldsymbol{x}) = \begin{bmatrix} {}_0\phi_i(\boldsymbol{x}) & 0 \\ 0 & {}_0\phi_i(\boldsymbol{x}) \end{bmatrix}, \tag{39}$$

$${}_0\boldsymbol{P}(\boldsymbol{x}) = \left({}_0\boldsymbol{P}_1(\boldsymbol{x}), {}_0\boldsymbol{P}_2(\boldsymbol{x}), \ldots, {}_0\boldsymbol{P}_n(\boldsymbol{x})\right), \tag{40}$$

$${}_0\boldsymbol{P}_i(\boldsymbol{x}) = \begin{bmatrix} {}_0\phi_i(\boldsymbol{x}) & 0 & 0 \\ 0 & {}_0\phi_i(\boldsymbol{x}) & 0 \\ 0 & 0 & {}_0\phi_i(\boldsymbol{x}) \end{bmatrix}, \tag{41}$$

and ϕ_i is the shape function of $\boldsymbol{x}$ with respect to node $\boldsymbol{x}_i$, which can be constructed by Eq. (27), ${}_0\boldsymbol{q}$ and ${}_0\boldsymbol{\beta}$ are the nodal incremental displacement vector and the nodal incremental stress vector, respectively,

$${}_0\boldsymbol{q}^{\mathrm{T}} = \left({}_0\boldsymbol{u}^{\mathrm{T}}(\boldsymbol{x}_1), {}_0\boldsymbol{u}^{\mathrm{T}}(\boldsymbol{x}_2), \ldots, {}_0\boldsymbol{u}^{\mathrm{T}}(\boldsymbol{x}_n)\right), \tag{42}$$

$${}_0\boldsymbol{u}(\boldsymbol{x}_i) = \begin{bmatrix} {}_0u_1(\boldsymbol{x}_i) \\ {}_0u_2(\boldsymbol{x}_i) \end{bmatrix}, \tag{43}$$

$$ {}_0\boldsymbol{\beta}^{\mathrm{T}} = \left({}_0\boldsymbol{\sigma}^{\mathrm{T}}(\boldsymbol{x}_1), {}_0\boldsymbol{\sigma}^{\mathrm{T}}(\boldsymbol{x}_2), \ldots, {}_0\boldsymbol{\sigma}^{\mathrm{T}}(\boldsymbol{x}_n)\right), \tag{44} $$

$$ {}_0\boldsymbol{\sigma}(\boldsymbol{x}_i) = \begin{bmatrix} {}_0\sigma_{11}(\boldsymbol{x}_i) \\ {}_0\sigma_{22}(\boldsymbol{x}_i) \\ {}_0\sigma_{12}(\boldsymbol{x}_i) \end{bmatrix}. \tag{45} $$

The matrix form of Eq. (4) in the two-dimensional problems is

$$ {}_0\boldsymbol{\varepsilon}(\boldsymbol{x}) = {}_0\boldsymbol{e}(\boldsymbol{x}) + {}_0\boldsymbol{\eta}(\boldsymbol{x}), \tag{46} $$

where

$$ {}_0\boldsymbol{e}(\boldsymbol{x}) = {}_0\boldsymbol{e}^{(\mathrm{L1})}(\boldsymbol{x}) + {}_0\boldsymbol{e}^{(\mathrm{L2})}(\boldsymbol{x}), \tag{47} $$

$$ {}_0\boldsymbol{e}^{(\mathrm{L1})}(\boldsymbol{x}) = \begin{bmatrix} {}_0u_{1,1} \\ {}_0u_{2,2} \\ {}_0u_{1,2} + {}_0u_{2,1} \end{bmatrix}, \tag{48} $$

$$ {}_0\boldsymbol{e}^{(\mathrm{L2})}(\boldsymbol{x}) = \begin{bmatrix} {}^t_0u_{1,1}{}_0u_{1,1} + {}^t_0u_{2,1}{}_0u_{2,1} \\ {}^t_0u_{1,2}{}_0u_{1,2} + {}^t_0u_{2,2}{}_0u_{2,2} \\ {}^t_0u_{1,1}{}_0u_{1,2} + {}^t_0u_{1,2}{}_0u_{1,1} \\ \quad + {}^t_0u_{2,1}{}_0u_{2,2} + {}^t_0u_{2,2}{}_0u_{2,1} \end{bmatrix}, \tag{49} $$

$$ \begin{aligned} {}_0\boldsymbol{\eta}(\boldsymbol{x}) &= \begin{bmatrix} {}_0\eta_{11}(\boldsymbol{x}) \\ {}_0\eta_{22}(\boldsymbol{x}) \\ 2{}_0\eta_{12}(\boldsymbol{x}) \end{bmatrix} \\ &= \frac{1}{2}\begin{bmatrix} ({}_0u_{1,1})^2 + ({}_0u_{2,1})^2 \\ ({}_0u_{1,2})^2 + ({}_0u_{2,2})^2 \\ 2({}_0u_{1,1}{}_0u_{1,2} + {}_0u_{2,1}{}_0u_{2,2}) \end{bmatrix}. \end{aligned} \tag{50} $$

Thus, equation (10) can be expressed as

$$ \begin{aligned} \prod_{\mathrm{HR}} = & \int_{{}_0\Omega} -\frac{1}{2}{}_0\boldsymbol{\sigma}^{\mathrm{T}}{}_0\boldsymbol{C}{}_0\boldsymbol{\sigma}^0 \mathrm{d}\Omega + \int_{{}_0\Omega} {}_0\boldsymbol{\sigma}^{\mathrm{T}}{}_0\boldsymbol{e}^0 \mathrm{d}\Omega \\ & + \int_{{}_0\Omega} {}_0\boldsymbol{e}^{\mathrm{T}}{}^t_0\boldsymbol{\sigma}^0 \mathrm{d}\Omega + \int_{{}_0\Omega} {}_0\boldsymbol{\eta}^{\mathrm{T}}{}^t_0\boldsymbol{\sigma}^0 \mathrm{d}\Omega \\ & - \int_{{}_0\Omega} {}^{t+\Delta t}_0\bar{\boldsymbol{F}}^{\mathrm{T}}{}_0\boldsymbol{u}^0 \mathrm{d}\Omega - \int_{{}_0\Gamma_\sigma} {}^{t+\Delta t}_0\bar{\boldsymbol{T}}^{\mathrm{T}}{}_0\boldsymbol{u}^0 \mathrm{d}\Gamma, \end{aligned} \tag{51} $$

where ${}_0\boldsymbol{C}$ can be obtained by Eqs. (13), (16), and (17).

Substitute Eqs. (36) and (37) into Eq. (51), we can obtain

$$ \begin{aligned} \Pi_{\mathrm{HR}} = & -\frac{1}{2}{}_0\boldsymbol{\beta}^{\mathrm{T}}\boldsymbol{H}{}_0\boldsymbol{\beta} + {}_0\boldsymbol{\beta}^{\mathrm{T}}\boldsymbol{G}{}_0\boldsymbol{q} + {}_0\boldsymbol{q}^{\mathrm{T}}\boldsymbol{Q}' \\ & + \frac{1}{2}{}_0\boldsymbol{q}^{\mathrm{T}}\boldsymbol{K}^{(\mathrm{NL})}{}_0\boldsymbol{q} - \boldsymbol{Q}^{\mathrm{T}}{}_0\boldsymbol{q}. \end{aligned} \tag{52} $$

Based on stationary value condition of multi-variation variation principle, i.e.,

$$ \frac{\partial \Pi_{\mathrm{HR}}({}_0\boldsymbol{\beta}, {}_0\boldsymbol{q})}{\partial {}_0\boldsymbol{\beta}} = 0, \tag{53} $$

and we can obtain

$$ {}_0\boldsymbol{\beta} = \boldsymbol{H}^{-1}\boldsymbol{G}{}_0\boldsymbol{q}. \tag{54} $$

Substituting Eq. (54) into Eq. (52), we obtain

$$ \begin{aligned} \Pi_{\mathrm{HR}}({}_0\boldsymbol{q}) = & \frac{1}{2}{}_0\boldsymbol{q}^{\mathrm{T}}\boldsymbol{K}^{(\mathrm{L})}{}_0\boldsymbol{q} + \frac{1}{2}{}_0\boldsymbol{q}^{\mathrm{T}}\boldsymbol{K}^{(\mathrm{NL})}{}_0\boldsymbol{q} \\ & + {}_0\boldsymbol{q}^{\mathrm{T}}\boldsymbol{Q}' - \boldsymbol{Q}^{\mathrm{T}}{}_0\boldsymbol{q}. \end{aligned} \tag{55} $$

According to the stationary condition of variation principle, i.e.,

$$ \frac{\partial \Pi_{\mathrm{HR}}({}_0\boldsymbol{q})}{\partial {}_0\boldsymbol{q}} = 0, \tag{56} $$

the following equations can be obtained:

$$ \left(\boldsymbol{K}^{(\mathrm{L})} + \boldsymbol{K}^{(\mathrm{NL})}\right){}_0\boldsymbol{q} = \boldsymbol{Q} - \boldsymbol{Q}', \tag{57} $$

where

$$ \boldsymbol{K}^{(\mathrm{L})} = \boldsymbol{G}^{\mathrm{T}}\boldsymbol{H}^{-1}\boldsymbol{G}, \tag{58} $$

$$ \boldsymbol{K}^{(\mathrm{NL})} = \int_{{}_0\Omega} {}_0\boldsymbol{B}^{(\mathrm{NL})\mathrm{T}}{}^t_0\hat{\boldsymbol{\sigma}}{}_0\boldsymbol{B}^{\mathrm{NL}0} \mathrm{d}\Omega, \tag{59} $$

$$ \boldsymbol{Q}^{\mathrm{T}} = \int_{{}_0\Omega} {}^{t+\Delta t}_0\bar{\boldsymbol{F}}^{\mathrm{T}}{}_0\boldsymbol{\Phi}^0 \mathrm{d}\Omega + \int_{{}_0\Gamma_\sigma} {}^{t+\Delta t}_0\bar{\boldsymbol{T}}^{\mathrm{T}}{}_0\boldsymbol{\Phi}^0 \mathrm{d}\Gamma, \tag{60} $$

$$ \boldsymbol{Q}' = \int_{{}_0\Omega} {}_0\boldsymbol{B}^{(\mathrm{L})\mathrm{T}}{}^t_0\boldsymbol{\sigma}^0 \mathrm{d}\Omega, \tag{61} $$

$$ \boldsymbol{G} = \int_{{}_0\Omega} {}_0\boldsymbol{P}^{\mathrm{T}}{}_0\boldsymbol{B}^{(\mathrm{L})0} \mathrm{d}\Omega, \tag{62} $$

$$ \boldsymbol{H} = \int_{{}_0\Omega} {}_0\boldsymbol{P}^{\mathrm{T}}{}_0\boldsymbol{C}{}_0\boldsymbol{P}^0 \mathrm{d}\Omega, \tag{63} $$

$$ {}_0\boldsymbol{B}^{(\mathrm{NL})}(\boldsymbol{x}) = \begin{bmatrix} \phi_{1,1}(\boldsymbol{x}) & 0 & \phi_{2,1}(\boldsymbol{x}) & 0 & \cdots & \phi_{n,1}(\boldsymbol{x}) & 0 \\ \phi_{1,2}(\boldsymbol{x}) & 0 & \phi_{2,2}(\boldsymbol{x}) & 0 & \cdots & \phi_{n,2}(\boldsymbol{x}) & 0 \\ 0 & \phi_{1,1}(\boldsymbol{x}) & 0 & \phi_{2,1}(\boldsymbol{x}) & \cdots & 0 & \phi_{n,1}(\boldsymbol{x}) \\ 0 & \phi_{1,2}(\boldsymbol{x}) & 0 & \phi_{2,2}(\boldsymbol{x}) & \cdots & 0 & \phi_{n,2}(\boldsymbol{x}) \end{bmatrix}, \tag{64} $$

$$ {}^t_0\hat{\boldsymbol{\sigma}} = \begin{bmatrix} {}^t_0\sigma_{11} & {}^t_0\sigma_{12} & 0 & 0 \\ {}^t_0\sigma_{12} & {}^t_0\sigma_{22} & 0 & 0 \\ 0 & 0 & {}^t_0\sigma_{11} & {}^t_0\sigma_{12} \\ 0 & 0 & {}^t_0\sigma_{12} & {}^t_0\sigma_{22} \end{bmatrix}, \tag{65} $$

$$ {}_0\boldsymbol{B}^{(\mathrm{L})}(\boldsymbol{x}) = {}_0\boldsymbol{B}^{(\mathrm{L1})}(\boldsymbol{x}) + {}_0\boldsymbol{B}^{(\mathrm{L2})}(\boldsymbol{x}), \tag{66} $$

$$ {}_0\boldsymbol{B}^{(\mathrm{I})}(\boldsymbol{x}) = \left({}_0\boldsymbol{B}^{(\mathrm{I})}_1(\boldsymbol{x}), {}_0\boldsymbol{B}^{(\mathrm{I})}_2(\boldsymbol{x}), \ldots, {}_0\boldsymbol{B}^{(\mathrm{I})}_n(\boldsymbol{x})\right), \tag{67} $$

$$ {}_0\boldsymbol{B}^{(\mathrm{L1})}_i(\boldsymbol{x}) = \begin{bmatrix} {}_0\phi_{i,1}(\boldsymbol{x}) & 0 \\ 0 & {}_0\phi_{i,2}(\boldsymbol{x}) \\ {}_0\phi_{i,2}(\boldsymbol{x}) & {}_0\phi_{i,1}(\boldsymbol{x}) \end{bmatrix}, \tag{68} $$

$$ {}_0\boldsymbol{B}^{(\mathrm{L2})}_i(\boldsymbol{x}) = \begin{bmatrix} L_{110}\phi_{i,1}(\boldsymbol{x}) & L_{210}\phi_{i,1}(\boldsymbol{x}) \\ L_{120}\phi_{i,2}(\boldsymbol{x}) & L_{220}\phi_{i,2}(\boldsymbol{x}) \\ L_{110}\phi_{i,2}(\boldsymbol{x}) + L_{120}\phi_{i,1}(\boldsymbol{x}) & L_{210}\phi_{i,2}(\boldsymbol{x}) + L_{220}\phi_{i,1}(\boldsymbol{x}) \end{bmatrix}, \tag{69} $$

$$L_{11} = {}^{t}_{0}u_{1,1} = \sum_{i=1}^{n} {}_{0}\phi_{i,1}(\boldsymbol{x})\,{}^{t}_{0}u_{1}(\boldsymbol{x}_i), \tag{70}$$

$$L_{12} = {}^{t}_{0}u_{1,2} = \sum_{i=1}^{n} {}_{0}\phi_{i,2}(\boldsymbol{x})\,{}^{t}_{0}u_{1}(\boldsymbol{x}_i), \tag{71}$$

$$L_{21} = {}^{t}_{0}u_{2,1} = \sum_{i=1}^{n} {}_{0}\phi_{i,1}(\boldsymbol{x})\,{}^{t}_{0}u_{2}(\boldsymbol{x}_i), \tag{72}$$

$$L_{22} = {}^{t}_{0}u_{2,2} = \sum_{i=1}^{n} {}_{0}\phi_{i,2}(\boldsymbol{x})\,{}^{t}_{0}u_{2}(\boldsymbol{x}_i). \tag{73}$$

The above is the HNEM for two-dimensional elasto-plastic large deformation problems. The Newton–Raphson method can be adopted to solve Eq. (57).

4. Numerical examples

In this section, several examples are presented to illustrate the applicability of the HNEM for two-dimensional elastoplastic large deformation problems. The results of these examples are obtained by using the HNEM, NEM, and Abaqus. Delaunay triangles are used as integration cells, gauss integration is adopted as integration scheme, and three Gauss points are used in each integration cell. The loads in these examples do not vary with the configuration of the object.

4.1. Cantilever beam with a concentrated force

Consider a cantilever beam subjected to a concentrated force, the left side is clamped, as shown in Fig. 3. The concentrated force is $p = 10$ N, length of the beam is $L = 10$ m, height is $H = 1$ m, and the unit thickness of the beam is considered. Elasticity modulus and Poisson's ratio are $E = 1.2 \times 10^4$ Pa and $\nu = 0.2$, respectively. The yield stress is $\sigma_s = 480$ Pa and $E' = 0.2E$. Regardless of the gravity, the beam can be discussed as a plane stress problem.

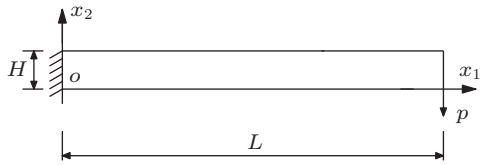


Fig. 3. Cantilever beam with a concentrated force.

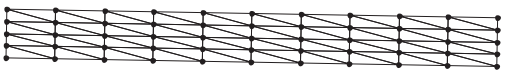


Fig. 4. Nodal distribution and Delaunay triangles of the cantilever beam.

As shown in Fig. 4, 55 nodes and 80 Delaunay triangles are distributed on the cantilever beam. One hundred steps are adopted to apply the load. The nodal vertical displacements, at the axis of the cantilever beam, are shown in Figs. 5 and 6. Under the same nodal layout, the results from the HNEM agree better with those from the Abaqus than the ones from the NEM, as shown in Fig. 5. Under a similar numerical precision, the CPU time used in the HNEM is less than that in the NEM, as shown in Fig. 6.

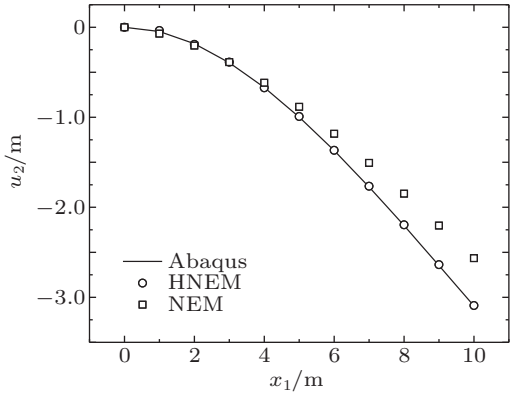


Fig. 5. Vertical displacements of the nodes at the axis of the cantilever beam.

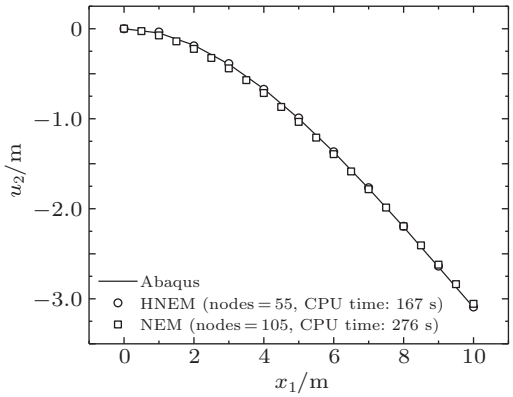


Fig. 6. Vertical displacements of the nodes at the axis of the cantilever beam and the comparison of the CPU time between the HNEM and the NEM.

4.2. Cylinder under a distributed inner pressure

A thick walled cylinder under a distributed inner pressure is considered, as shown in Fig. 7. The inner pressure is $p = 1000$ Pa, and the radiuses are $a = 1$ m and $b = 5$ m. The elasticity modulus and Poisson ratio are $E = 1.0 \times 10^5$ Pa and $\nu = 0.25$, respectively. The yield stress is $\sigma_s = 150$ Pa, and $E' = 0.2E$. The cylinder can be discussed as a plane strain problem without considering the body force.

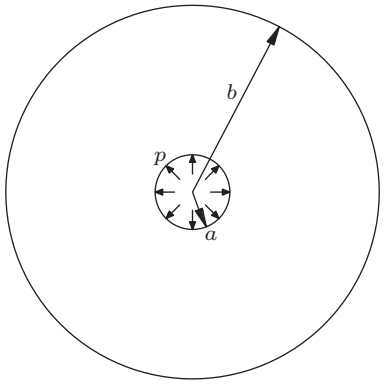


Fig. 7. Cylinder under a distributed inner pressure.

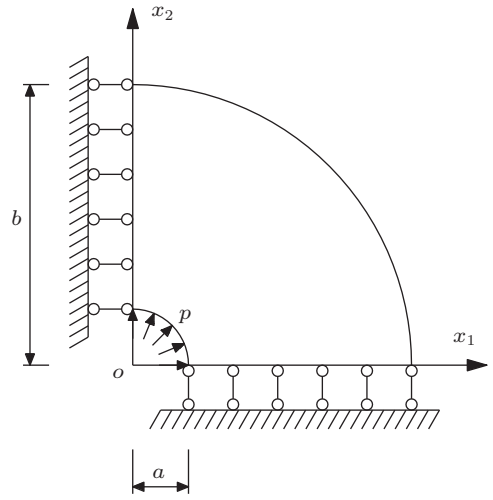


Fig. 8. A quarter of the cylinder with boundary conditions.

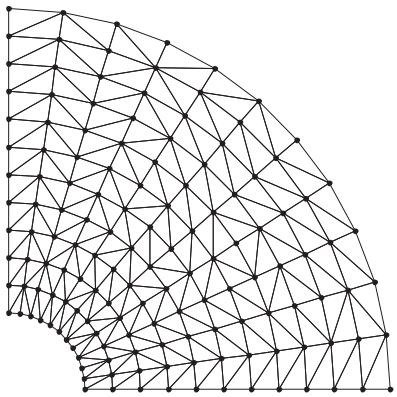


Fig. 9. Nodal distribution and Delaunay triangles of a quarter of the cylinder.

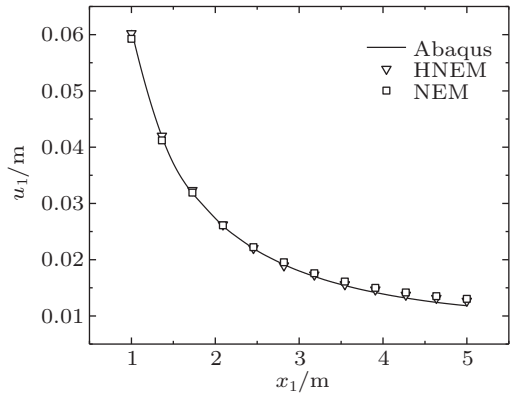


Fig. 10. Horizontal displacements of nodes at $x_2 = 0$ of the cylinder.

Consider the symmetry of the cylinder, only a quarter of the cylinder needs to be calculated, as shown in Fig. 8. Figure 9 shows 144 nodes with corresponding Delaunay triangles used for solution. The number of the whole load steps is set as 100. The nodal horizontal displacements at $x_2 = 0$ obtained using the HNEM and NEM are shown in Fig. 10. It can be seen that, under the condition of the same nodal layout, the results attained by the HNEM are closer to that using Abaqus than ones using the NEM.

4.3. Square plate with a central hole subjected to an axial uniform tension

A square plate with a central hole subjected to an axial uniform tension is shown in Fig. 11. The axial uniform tension is $q = 1000$ N/m, the length is $L = 10$ m, and the radius of the hole is $R = 1$ m. The elasticity modulus and Poisson ratio are $E = 1.0 \times 10^5$ Pa and $\nu = 0.25$, respectively. The yield stress is $\sigma_s = 400$ Pa and $E' = 0.2E$. The unit thickness of the plate is considered. Regardless of the body force, the plate can be calculated as a plane stress problem.

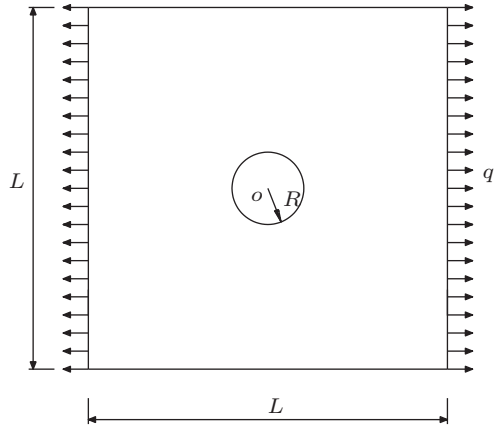


Fig. 11. A square plate with a central hole subjected to an axial uniform tension.

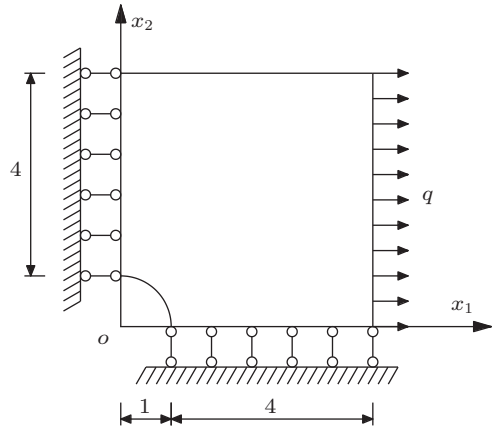


Fig. 12. A quarter of the square plate with boundary conditions.

As shown in Fig. 12, only a quarter of the square plate needs to be considered. 99 nodes and the corresponding Delaunay triangles are distributed on a quarter of the square plate, as shown in Fig. 13. 200 steps are adopted to apply the load. With the same nodal distribution, the nodal horizontal displacements of the plate at $x_2 = 5$ m obtained from the HNEM and the NEM are shown in Fig. 14. It can be observed that the results from the HNEM are in better agreement with the ones from the Abaqus than those from the NEM.

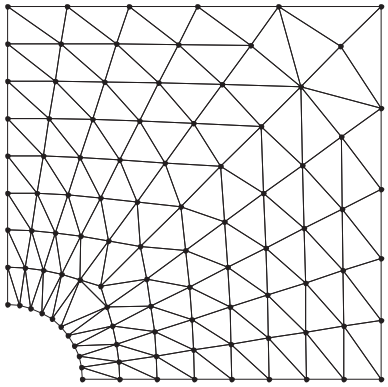


Fig. 13. Nodal distribution and Delaunay triangles of a quarter of the square plate.

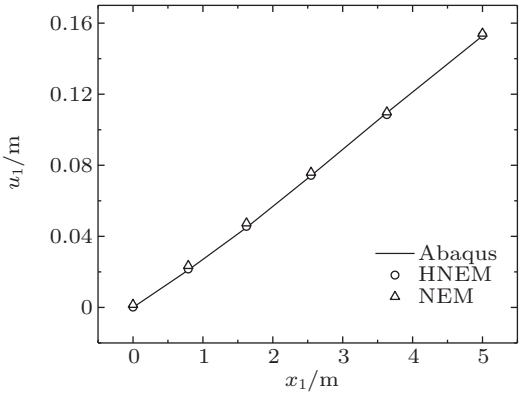


Fig. 14. Nodal horizontal displacements of the plate at $x_2 = 5$ m.

4.4. Clamped beam under a distributed load

The final example is a beam, which is fixed at both ends and subjected to a distributed load, as shown in Fig. 15. The length of the beam is $L = 10$ m, height is $H = 1$ m, and the unit thickness of the beam is considered. The distributed load is $p = 50$ N/m. The elasticity modulus is $E = 1.2 \times 10^4$ Pa, Poisson's ratio is $\nu = 0.2$, the yield stress is $\sigma_s = 480$ Pa, and $E' = 0.2E$. The beam can be discussed as a plane stress problem without considering the gravity.

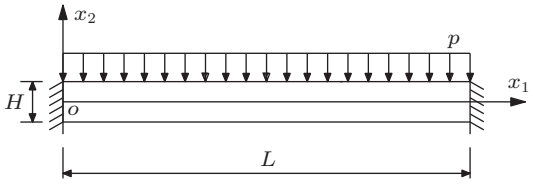


Fig. 15. Clamped beam under a distributed load.

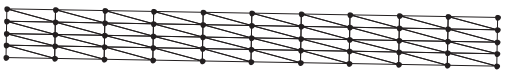


Fig. 16. Nodal distribution and Delaunay triangles of the clamped beam.

We adopt 55 nodes and 80 Delaunay triangles for this example, as shown in Fig. 16. The number of load steps is 100. The vertical displacements of nodes at the axis of the beam obtained by the HNEM and NEM are shown in Figs. 17 and 18. From Fig. 17, we can see that, under the same nodal distribution, the results obtained by using the HNEM agree better with the ones using the Abaqus than the ones using the NEM. It can be observed from Fig. 18 that the CPU time spent in the HNEM is less than that in the NEM under a similar numerical precision. This demonstrates that the HNEM has a higher computational efficiency than the NEM.

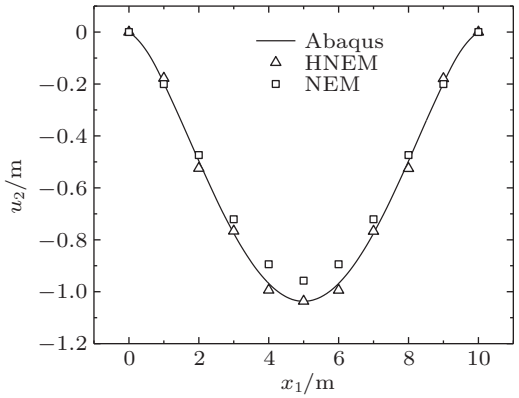


Fig. 17. Vertical displacements of the nodes at the axis of the clamped beam.

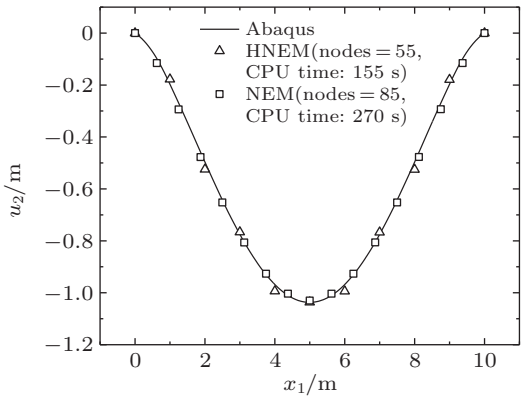


Fig. 18. Vertical displacements of the nodes at the axis of the clamped beam and the comparison of the CPU time between the HNEM and the NEM.

5. Conclusions

The HNEM for analyzing large deformation elastoplasticity problems is discussed in this paper. The Sibson interpolation shape functions are chosen as the trial and test functions of nodal incremental displacements and incremental stresses. The incremental formulation of Hellinger–Reissner variational principle suitable for elastoplastic large deformation problems is deduced to obtain the incremental discrete equations, and these equations are solved by the Newton–Raphson iteration method. Some numerical examples of large deformation elastoplasticity problems show that the results of the HNEM have higher computational precision and efficiency than the ones of the NEM.

References

[1] Onishi Y and Amaya K 2012 *Int. J. Numer. Meth. Eng.* **92** 36
[2] Belytschko T, Lu Y Y and Gu L 1994 *Int. J. Numer. Meth. Eng.* **37** 229
[3] Wang J F, Sun F X and Cheng R J 2010 *Chin. Phys. B* **19** 060201
[4] Cheng R J and Cheng Y M 2011 *Chin. Phys. B* **20** 070206
[5] Zhang Z, Liew K M and Cheng Y 2008 *Engin. Anal. Bound. Elem.* **32** 100
[6] Zhang Z, Liew K M, Cheng Y and Lee Y Y 2008 *Engin. Anal. Bound. Elem.* **32** 241
[7] Zhang Z, Hao S Y, Liew K M and Cheng Y M 2013 *Engin. Anal. Bound. Elem.* **37** 1576
[8] Zhang Z, Wang J, Cheng Y and Liew K M 2013 *Sci. China-Phys. Mech. Astron.* **56** 1568
[9] Cheng Y M and Li J H 2005 *Acta Phys. Sin.* **54** 4463 (in Chinese)
[10] Wang J F and Cheng Y M 2012 *Chin. Phys. B* **21** 120206
[11] Wang J F and Cheng Y M 2013 *Chin. Phys. B* **22** 030208
[12] Peng M J, Liu P and Cheng Y M 2009 *Int. J. Appl. Mech.* **1** 367
[13] Peng M J, Li D M and Cheng Y M 2011 *Eng. Struct.* **33** 127
[14] Bai F N, Li D M, Wang J F and Cheng Y M 2012 *Chin. Phys. B* **21** 020204
[15] Cheng Y M, Wang J F and Bai F N 2012 *Chin. Phys. B* **21** 090203
[16] Cheng Y M, Wang J F and Li R X 2012 *Int. J. Appl. Mech.* **4** 1250042
[17] Ren H P and Cheng Y M 2011 *Int. J. Appl. Mech.* **3** 735
[18] Ren H P and Cheng Y M 2012 *Eng. Anal. Bound. Elem.* **36** 873
[19] Dai B D and Cheng Y M 2007 *Acta Phys. Sin.* **56** 597 (in Chinese)
[20] Cheng R J and Cheng Y M 2007 *Acta Phys. Sin.* **56** 5569 (in Chinese)
[21] Wang J F, Bai F N and Cheng Y M 2011 *Chin. Phys. B* **20** 030206
[22] Atluri S N and Zhu T 1998 *Comput. Mech.* **22** 117
[23] Chen L and Cheng Y M 2008 *Acta Phys. Sin.* **57** 1 (in Chinese)
[24] Chen L and Cheng Y M 2008 *Acta Phys. Sin.* **57** 6047 (in Chinese)
[25] Chen L and Cheng Y M 2010 *Chin. Phys. B* **19** 090204
[26] Chen L, Ma H P and Cheng Y M 2013 *Chin. Phys. B* **22** 050202
[27] Weng Y J and Cheng Y M 2013 *Chin. Phys. B* **22** 090204
[28] Li S C, Cheng Y M and Li S C 2006 *Acta Phys. Sin.* **55** 4760 (in Chinese)
[29] Gao H F and Cheng Y M 2010 *Int. J. Comput. Methods* **7** 55
[30] Cheng Y M and Chen M J 2003 *Acta Mech. Sin.* **35** 181 (in Chinese)
[31] Cheng Y M and Peng M J 2005 *Sci. Chin. Ser. G: Phys. Mech. Astron.* **48** 641
[32] Kitipornchai S, Liew K M and Cheng Y M 2005 *Comput. Mech.* **36** 13
[33] Liew K M, Cheng Y M and Kitipornchai S 2005 *Int. J. Numer. Methods Eng.* **64** 1610
[34] Liew K M, Cheng Y M and Kitipornchai S 2006 *Int. J. Numer. Methods Eng.* **65** 1310
[35] Liew K M, Cheng Y M and Kitipornchai S 2007 *Int. J. Solids Struct.* **44** 4220
[36] Cheng Y M, Liew K M and Kitipornchai S 2009 *Int. J. Numer. Methods Eng.* **78** 1258
[37] Liew K M and Cheng Y M 2009 *Comput. Meth. Appl. Mech. Eng.* **198** 3925
[38] Peng M J and Cheng Y M 2009 *Eng. Anal. Bound. Elem.* **33** 77
[39] Ren H P, Cheng Y M and Zhang W 2009 *Chin. Phys. B* **18** 4065
[40] Ren H P, Cheng Y M and Zhang W 2010 *Sci. China-Phys. Mech. Astron.* **53** 758
[41] Wang J F, Sun F X and Cheng Y M 2012 *Chin. Phys. B* **21** 090204
[42] Wang J F, Wang J F, Sun F X and Cheng Y M 2013 *Int. J. Comput. Methods* **10** 1350043
[43] Braun J and Sambridge M 1995 *Nature* **376** 655
[44] Sukumar N, Moran B and Belytschko T 1998 *Int. J. Numer. Methods Eng.* **43** 839
[45] Bueche D, Sukumar N and Moran B 2000 *Comput. Mech.* **25** 207
[46] Cueto E, Calvo B and Doblare M 2002 *Int. J. Numer. Methods Eng.* **54** 871
[47] Martínez M, Cueto E, Doblaré M and Chinesta F 2003 *J. Non-Newton. Fluid Mech.* **115** 51
[48] Calvo B, Martinez M A and Doblaré M 2005 *Int. J. Numer. Methods Eng.* **62** 159
[49] Daneshmand F and Niroomandi S 2007 *Eng. Comput.* **24** 269
[50] Daneshmand F, Javanmard S S, Liaghat T, Moshksar M M and Adamowski J F 2010 *Can. J. Civ. Eng.* **37** 1550
[51] Shahrokhabadi S, Toufigh M M and Gholizadeh R 2010 *GeoShanghai International Conference - Geoenvironmental Engineering and Geotechnics*, June 3-5, 2010 Shanghai, China, p. 245
[52] Cho J R, Lee H W and Yoo W S 2013 *Comput. Meth. Appl. Mech. Eng.* **256** 17
[53] Dong Y, Ma Y Q and Feng W 2012 *Acta Mech. Sin.* **44** 568 (in Chinese)
[54] Ma Y Q, Dong Y, Zhou Y K and Feng W 2014 *Math. Probl. Eng.* **2014** 9
[55] Chen J S, Pan C H, Wu C T and Liu W K 1996 *Comput. Meth. Appl. Mech. Eng.* **139** 195
[56] Li S F, Hao W and Liu W K 2000 *Int. J. Solids Struct.* **37** 7185
[57] Ren J, Liew K M and Meguid S A 2002 *Int. J. Mech. Sci.* **44** 2393
[58] Liew K M, Ren J and Kitipornchai S 2004 *Eng. Anal. Bound. Elem.* **28** 497
[59] Liew K M, Peng L X and Kitipornchai S 2007 *Comput. Meth. Appl. Mech. Eng.* **196** 2358
[60] Naffa M and Al-Gahtani H J 2007 *Eng. Anal. Bound. Elem.* **31** 311
[61] Rossi R and Alves M 2007 *Comput. Mech.* **39** 381
[62] Zhao X and Liew K M 2009 *Comput. Meth. Appl. Mech. Eng.* **198** 2796
[63] Doweidar M H, Calvo B, Alfaro I, Groenenboom P and Doblaré M 2010 *Comput. Meth. Appl. Mech. Eng.* **199** 1691
[64] Li D M, Bai F N, Cheng Y M and Liew K M 2012 *Comput. Meth. Appl. Mech. Eng.* **233** 1
[65] Li D M, Liew K M and Cheng Y M 2014 *Comput. Meth. Appl. Mech. Eng.* **269** 72
[66] Li D M, Liew K M and Cheng Y M 2014 *Comput. Mech.* **53** 1149
[67] Peng L X, Tao Y P, Li H Q and Mo G K 2014 *Math. Probl. Eng.* **2014** 548708
[68] Pian T H H 1976 *J. Frankl. Inst. - Eng. Appl. Math.* **302** 473